Unusual dimerization and magnetization plateaus in $S = 1$ skew chain $Ni_2V_2O_7$ observed at 120 T

J. J. Cao,[1] Z. W. Ouyang,[1,*] X. C. Liu,[1] T. T. Xiao,[1] Y. R. Song,[1] J. F. Wang,[1,†] Y. Ishii,[2] X. G. Zhou,[2] and Y. H. Matsuda[2,‡]

[1]*Wuhan National High Magnetic Field Center & School of Physics, Huazhong University of Science and Technology, Wuhan 430074, People's Republic of China*

[2]*Institute for Solid State Physics, University of Tokyo, Kashiwa, Chiba 277-8581, Japan*

(Received 1 August 2022; accepted 24 October 2022; published 9 November 2022)

Using ultrahigh magnetic field up to 120 T, a 1/2 magnetization plateau within 11.7–34.8 T and a 3/4-like plateau within 55.6–87.0 T have been observed in the *S*-1 skew chain antiferromagnet $Ni_2V_2O_7$. By combining density functional theory calculations, exact diagonalization, and quantum Monte Carlo simulations, we find that the nearest-neighbor interchain interaction ($J_3/k_B = -78.5$ K) is much stronger than the intrachain interactions ($J_1/k_B = -1.0$ K and $J_2/k_B = 6.3$ K), showing surprising "dimerization" of magnetic ions caused by the large 3*d*-orbital overlap along the Ni1-Ni1 bond. Thus a "dimer+monomer" model is proposed to describe the magnetization process—the 1/2 plateau pertains to weakly coupled Ni2 monomers while the 3/4-like plateau to the strongly coupled Ni1 dimers. The possible supersolid phases from the Ni1 dimers are proposed.

DOI: 10.1103/PhysRevB.106.184409

I. INTRODUCTION

Quantum magnetism and its interplay with topological structure are of particular interesting. Representative examples are the spin Peierls effect and the formation of clusters in many antiferromagnetic (AFM) spin systems such as one-dimensional (1D) chain $NaTiSi_2O_6$ [1], triangular lattice $LiVO_2$ [2], kagome lattice $LiZn_2Mo_3O_8$ [3,4], and spinel lattice $MgTi_2O_4$ [5] driven by particular orbital order. Recently, the volborthite kagome compound $Cu_3V_2O_7(OH)_2{\cdot}2H_2O$ [6,7] was described as coupled trimmers rather than frustrated chains. The $S = 1$ kagome antiferromagnet $Na_2Ti_3Cl_8$ was reported to present a trimerized phase [8], which actually corresponds to dimerization in all three directions [9] due to the "orbital-driven" Peierls effect. Reduction of dimensionality and clusterization-related physics [10] renew interests in quantum magnets.

In this paper, we report a fascinating "dimerization" in the skew chain compound $Ni_2V_2O_7$, which leads to wide 1/2 and 3/4-like magnetization plateaus revealed in ultrahigh fields of up to 120 T. Magnetization plateau, at which magnetization remains unaltered in a certain magnetic field range, is known to exist in many antiferromagnet with triangular [11–13], kagome [14–17], as well as other frustrated lattices [18–20]. $Ni_2V_2O_7$ is a skew chain antiferromagnet. As shown in Fig. 1(a), the edge-shared $Ni1O_6$ and $Ni2O_6$ octahedra are linked alternatively, forming skew chains along the *c* axis [21]. The adjacent chains are connected with each other by the $Ni1O_6$ octahedra. Magnetically, $Ni_2V_2O_7$ is a 3D antiferromagnet with long-range ordering at $T_N = 7$ K and spin-flop-like transitions at low fields [22]. For such a classical antiferromagnet, one takes it for granted that above the spin-flop transition the magnetization will increase linearly until saturation. However, we recently observed a wide 1/2 magnetization plateau within 8–30 T [23,24], which is difficult to understand. The $S = 1$ bond-alternating chain model could provide a dimer phase and 1/2 magnetization plateau [25–27], but fails to produce a magnetic ground state and a wide 1/2 plateau. Hence, a triangular-like tetramer model was proposed to interpret the 1/2 plateau, and the roles of magnetic frustration and interchain interactions were emphasized [23]. However, the estimated interchain interaction is not dominant over the intrachain interactions, in contrast to the results of theoretical calculations [28]. The 1/2 magnetization plateau in $Ni_2V_2O_7$ remains puzzling.

Puzzled by the wide 1/2 plateau, we have measured the ultrahigh field magnetization of $Ni_2V_2O_7$ up to 120 T. Intriguingly, in addition to the wide 1/2 plateau within 11.7–34.8 T, a new and wider 3/4-like plateau within 55.6–87.0 T is observed. Density functional theory (DFT), exact diagonalization (ED) and quantum Monte Carlo (QMC) simulation are utilized to interpret the plateaus. The results suggest a significant "dimerization" of magnetic ions driven by particular orbital overlap along the Ni1-Ni1 bond. $Ni_2V_2O_7$ is an antiferromagnet composed of Ni1 dimers plus Ni2 monomers [see Fig. 1(b)] rather than 1D chain magnet [see Fig. 1(a)].

II. EXPERIMENT DETAILS

Polycrystalline sample of $Ni_2V_2O_7$ [28] was used for the experiments because single crystals with large sizes are not available to conduct an ultrahigh field measurement. This is acceptable because our previous study showed that the anisotropy of high-field magnetization including the 1/2 plateau is very small [23]. Pulsed high-field $M(H)$ curve at

*zwouyang@mail.hust.edu.cn
†jfwang@hust.edu.cn
‡ymatsuda@issp.u-tokyo.ac.jp

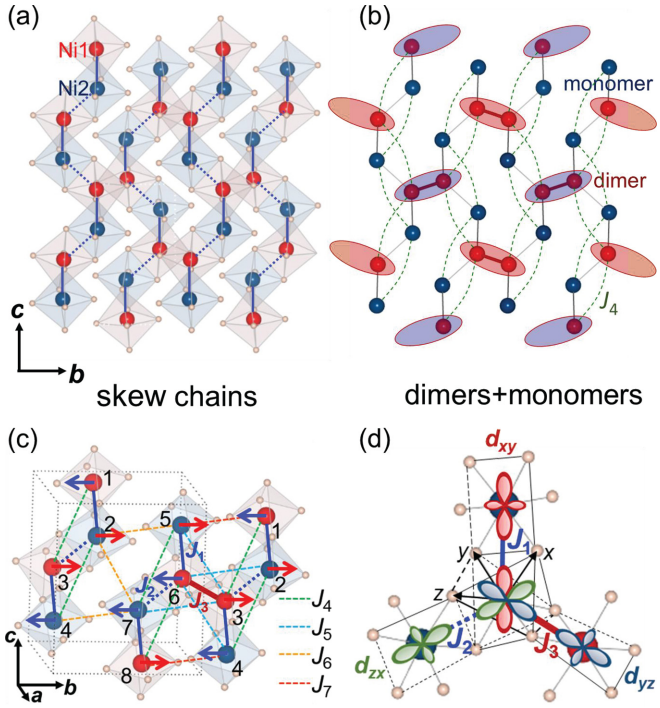

FIG. 1. (a) Skew chain structure along the c axis. (b) "Dimers+monomers" model, in which dimers formed by the edge-sheared $Ni1O_6$ octahedra are highlighted with two different shaded ovals. (c) Exchange parameters considered in the DFT calculations: the NN intrachain J_1 (3.0095 Å), J_2 (3.0493 Å), and interchain J_3 (2.9352 Å) as well as the other intrachain J_4 and interchain J_5-J_7. The ground-state spin configurations are shown by the arrows. (d) The NN superexchange paths: J_1—Ni1-O2-Ni2 (95.313°) and Ni1-O6-Ni2 (95.253°), J_2—Ni1-O3-Ni2 (94.411°) and Ni1-O4-Ni2 (95.567°) and J_3—Ni1-O7-Ni1 (98.696°). Local coordinate axes (x, y, z) and three t_{2g} orbitals (d_{xy}, d_{yz}, d_{zx}). For the central Ni1 ions, six lobes, i.e., two of the four lobes for each of the three t_{2g} orbitals are drawn, and for the three peripheral ions, only pertinent orbitals (d_{yz} for Ni1, d_{xy} and d_{zx} for Ni2) are drawn.

54 T was measured by a standard inductive method at Wuhan National High Magnetic Field Center, China. Ultrahigh field $M(H)$ measurements were performed at Institute for Solid State Physics, University of Tokyo, Japan. The pulsed magnetic field of up to 120 T was generated by a destructive method using single-turn coil technique, details of which can be found in Refs. [29,30].The magnetic susceptibility $\chi(T)$ and low-field $M(H)$ used to calibrate the high-field data were measured using a commercial physical property measurement system (16-T PPMS).

III. RESULTS AND DISCUSSION

A. Experimental results

Figure 2(a) shows the $M(H)$ and its dM/dH curves measured in the up-sweeping process at 120 T and 4.5 K, as well as the 54 T data at 4.2 K for comparison. The data for the down-sweeping process are not presented because the measurement is rather imprecise due to the field inhomogeneity caused by mechanical deformation of the coil. The $M(H)$ curve exhibits series of field-induced magnetic

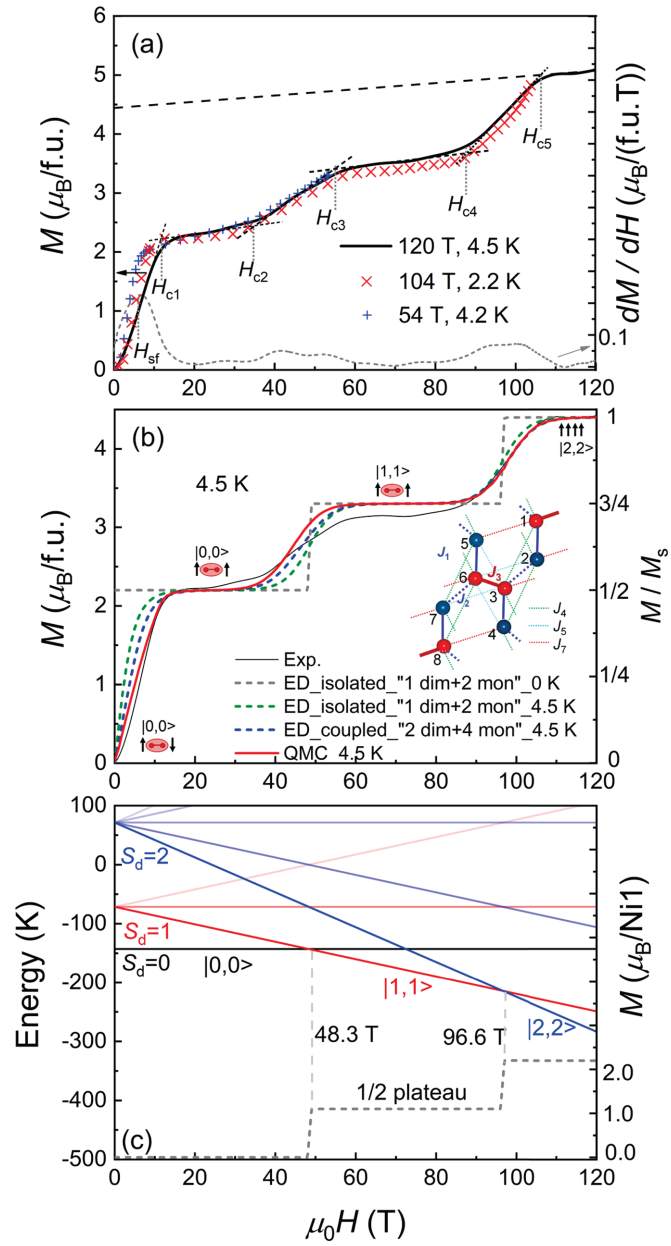

FIG. 2. (a) $M(H)$ curve and its dM/dH at 120 T (4.5 K). The 104 T (2.2 K) and 54 T (4.2 K) data are also shown for comparison. The critical fields, H_{c1}–H_{c5}, are defined by intersections of linear extrapolations of adjacent curves. (b) ED- and QMC-simulated $M(H)$ curves, the experimental $M(H)$ and normalized M/M_s curves at 120 T corrected for the van Vleck term. Schematic representations of spin states are also shown, where the dimer states are highlighted (shaded ovals). (c) Energy levels as a function of magnetic field and the 1/2 magnetization plateau for an isolated Ni1 dimer ($J_3 = -71.4$ K and $g = 2.2$).

transitions, which reflects that the temperature change of the sample due to semiadiabatic magnetization process is small or negligible. Otherwise, if sample temperature is elevated to 6 K ($T_N = 7$ K) the magnetic transitions will disappear [24]. Since dM/dH presents too many peaks, the critical fields are not defined by dM/dH but by intersections of linear extrapolations of adjacent curves. It can be seen that the $M(H)$ curve

below 54 T exhibits a low-field spin-flop-like transition, a 1/2 plateau between $H_{c1} = 11.7$ T and $H_{c2} = 34.8$ T, followed by a linear increase in magnetization, similar to the result up to 54 T at 4.2 K and that the previously reported up to 55 T at 2.0 K [23]. Further increasing the magnetic field, the $M(H)$ curve presents a new plateau between $H_{c3} = 55.6$ T and $H_{c4} = 87.0$ T with a width of $\Delta H = 31.4$ T, which is larger than that of the 1/2 plateau ($\Delta H = 23.1$ T). Above H_{c4}, the magnetization increases linearly until full saturation at $H_{c5} = 106.2$ T.

We also attempt to conduct the magnetization measurement at 2.2 K with field up to 104 T. As expected, the magnetization plateaus are more flat than the 4.5 K data [see Fig. 2(a)]. The small difference of H_{c1} can be attributed to the measurement temperature. The value of $H_{c1} = 6.6$ T for the $M(H)$ curve at 54 T is much lower than $H_{c1} = 11.7$ T for the curve at 120 T, reflecting that the magnetization process around H_{c1} is dynamic and is field-sweep-rate dependent. The average field sweep rate of the 54 T field is about 1×10^4 T/s, while that of the 120 T is about 4×10^7 T/s. A larger field sweep rate tends to move H_{c1} toward higher field. In the following analysis, we use the 120 T data reaching magnetic saturation.

The $M(H)$ curve at 120 T has a small slope in the magnetic saturation region [Fig. 2(a)] due to the contribution from van Vleck paramagnetism [12], which is estimated as $\chi_{VV} = 0.0054\,\mu_B$/(f.u.T). By substracting this term, the $M(H)$ curve is corrected and depicted in Fig. 2(b). Thus the saturated magnetization is estimated as $M_s = 4.4\,\mu_B$/f.u. expected for $S = 1$ and $g = 2.2$. The magnetization at the new plateau is about $3.15\,\mu_B$/f.u., close to 3/4 M_s. Thus, in addition to the 1/2 plateau, our 120 T experiment reveals a new 3/4-like plateau.

As stated above, the magnetization process containing wide 1/2 plateau is far from being understood with theoretical models previously proposed [23]. The new 3/4-like plateau brings us new challenges. Next, we discuss the appropriate model based on precise exchange parameters, which are of vital importance for understanding the magnetization process.

B. DFT calculations

To obtain precise exchange parameters, we perform DFT calculations with the full-potential code WIEN2K [31] by considering more spin configurations and exchange parameters than before [28]. We take $U_{eff} = U - J$, where U and J are on-site Coulomb term and exchange interactions, respectively [32]. Figure 1(c) depicts seven exchange interactions considered: the nearest-neighbor (NN) $J_1 - J_3$ and the next-nearest-neighbor (NNN) $J_4 - J_7$. Details on the calculations can be found in the Supplemental Material [33] (see, also, references [21,31,32,34–38] therein). The ground state of $Ni_2V_2O_7$ is determined, in which J_1 and J_3 is AFM whereas J_2 is ferromagnetic (FM) [see Fig. 1(c)]. By mapping the total energies of the eight spin configurations onto the spin Heisenberg model $\hat{H} = -\sum_{i,j} J_{i,j} \hat{S}_i \cdot \hat{S}_j$, the exchange parameters are deduced and summarized in Table I. Not depending on the choice of U_{eff}, the NN interchain J_3 is undoubtedly AFM, but its value is surprisingly large compared with the NN intrachain J_1 and J_2 and other four interactions. This suggests that the Ni1 ions are dimerized heavily and, on the contrary, the Ni2 ions behave like monomers.

TABLE I. Bond lengths (Å) and exchange interactions (K) for different U_{eff} (eV).

		J (DFT+U)			
	$d_{Ni\text{-}Ni}$	$U_{eff} = 0$	3	6	9
J_1/k_B	3.0095	−52.2	−14.1	−3.9	−1.0
J_2/k_B	3.0493	6.3	11.8	9.2	6.4
J_3/k_B	2.9352	−490.5	−241.2	−132.1	−80.0
J_4/k_B	5.1406	−9.0	−4.2	−2.3	−1.5
	5.1978				
J_5/k_B	5.1853	3.8	0.2	−0.5	−0.4
	5.1930				
J_6/k_B	4.8607	15.5	8.3	5.0	3.1
	4.9153				
	4.9272				
	4.9664				
J_7/k_B	5.0768	1.7	6.5	5.5	4.1
	5.1018				

The large J_3 leading to dimerization is counterintuitive. From the bond lengths and angles (see the caption of Fig. 1), the interchain J_3 should be the largest (the Ni1-Ni1 bond is the shortest). But the differences in bond lengths and angles are small, which means that J_1, J_2, and J_3 should be marginally different in size. Similar situation exists in the kagome lattice $Cu_3V_2O_7(OH)_2{\cdot}2H_2O$ [14–16], in which Cu trimers are formed, although the Cu-Cu distances and the Cu-O-Cu angles are very similar [6,7]. The orbital transition [39] was proposed to dramatically modify the magnetic interactions between Cu ions. In $Ni_2V_2O_7$, however, there are no orbital degrees of freedom for the Ni ions ($3d^8$). The possibility of spin-Peierls effect between the Ni1 ions can be ruled out, because at least our $\chi(T)$ curve (see below) does not exhibit a typical spin-Peierls transition.

As shown in Fig. 1, there are two different superexchange paths with slightly different bond angles for J_1 and J_2, while the two exchange paths are identical for J_3. With this difference, the orbital arrangements will be different, in spite of the absence of orbital order. We plot in Fig. 3 the density of states (DOS) for Ni-3d and O-2p and orbital-decomposed partial DOS of Ni-3d for no spin-polarization calculation. As expected for Ni ($3d^8$), the three low t_{2g} orbitals are nearly occupied completely, while the two high orbitals e_g are partially occupied. Within -1.7– -0.8 eV, d_{xy} (or d_{zx}) overlaps partially between Ni1 and Ni2, while d_{yz} overlaps completely between the two Ni1 ions [Fig. 1(d)], which renders J_3 much stronger than J_1 and J_2, leading to dimerization of Ni1 ions. Such large 3d-orbital overlap along the Ni1-Ni1 bond would enhance magnetic couplings, leading to reduction of dimensionality and clusterization of the system. This is different from the formation of clusters in many systems with orbital degrees of freedom [10].

C. ED and QMC simulations

Based on the DFT ($U_{eff} = 9$ eV) results, we have simulated the $M(H)$ curve at 120 T with ED and QMC methods by

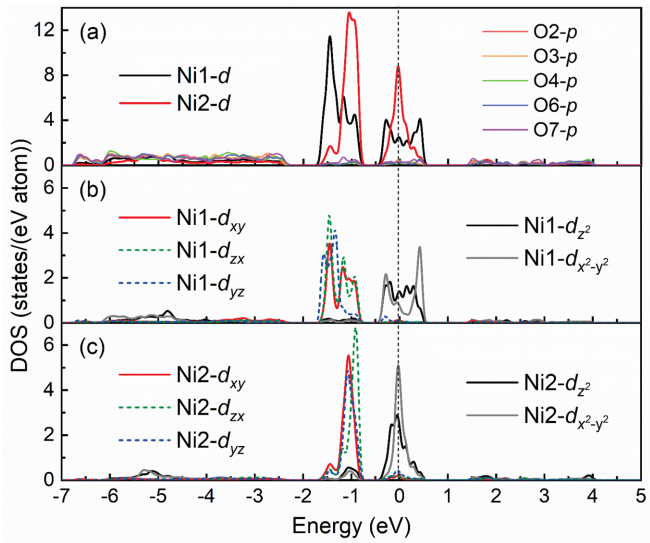

FIG. 3. (a) DOS for Ni-3*d* and O-2*p*. (b-c) Orbital-decomposed DOS for Ni-3*d*. The Fermi energy (dotted vertical line) is zero energy.

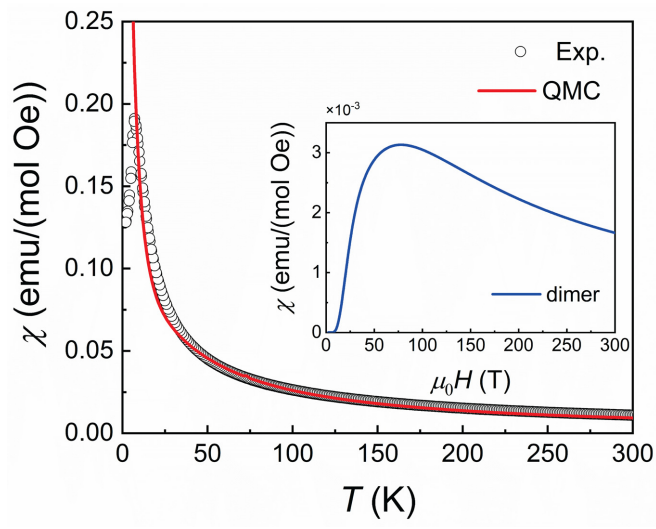

FIG. 4. QMC-simulated $\chi(T)$ curve and the experimental curve. The inset is the contribution from Ni1 dimers.

including the dominant J_3 and other six exchanges (Table I). To avoid over-parameterization, the ratio of exchange parameters J_1, J_2, and J_4 – J_7 is fixed. We thus have only two adjustable parameters J_3 and $k = |J_1/J_3|$. Details on the simulations are described in Ref. [33].

First, we consider only the leading J_3 and ignore the other interactions ($k = 0$), i.e., isolated "1 dimer + 2 monomers" mode at 0 K. Surprisingly, Fig. 2(b) shows that the calculated $M(H)$ curve (gray dashed line) with $J_3/k_B = -71.4$ K and $g = 2.2$ captures well the feature of the magnetization process—wide 1/2 and 3/4-like plateaus. When the temperature increases from 0 to 4.5 K, the ED-simulated curve (green dashed line) gives a good description for the magnetization process. In particular, the curve between H_{c4} and H_{c5} follows well the experimental data. Note that the low-field curve is not only related to temperature, but also to the field sweep rate [see Fig. 2(a)].

Next, we consider coupled "2 dimer+4 monomers" mode with J_3 and other interactions ($k \neq 0$) at 4.5 K. As seen from the blue dashed line in Fig. 2(b), the simulation is slightly improved compared with the isolated "1 dimer + 2 monomers" mode, but the effect of single ion anisotropy D can be ignored [33]. By the QMC method with more spin number, the simulated curve (red solid line) gives a better description for the magnetization process expect for the small discrepancy in the 3/4-like plateau region. Similar discrepancy was observed in $Co_2V_2O_7$ [40]. The QMC simulation yields exchange parameters: $J_3/k_B = -78.5$ K and $J_1/k_B = -1.0$ K, $J_2/k_B = 6.3$ K, $J_4/k_B = -1.5$ K, $J_5/k_B = -0.4$ K, $J_6/k_B = 5.4$ K, and $J_7/k_B = -0.2$ K ($k = 1/80$). There is marginal difference between the QMC and the DFT ($U_{eff} = 9$ eV) results. From the mean-field model, the Curie-Weiss temperature is calculated as $\theta_{CW} = -30.3$ K, close to the experimental value of $\theta_{CW} = -25.0$ K [22].

Based on the results above, we propose a "dimer+monomer" model—$Ni_2V_2O_7$ is an antiferromagnet composed of strongly antiferromagnetically coupled Ni1 dimers and weakly interacting Ni2 monomers [see Fig. 1(b)]. The weakly interacting Ni2 monomers drive the system to be long-range ordered at $T_N = 7$ K. In the magnetization process below T_N, the AFM Ni2 ions along the chain [see J_4 in Fig. 1(c)] are first responsible for the low-field spin-flop-like transition at H_{sf}, and then they will be magnetized to saturation quickly under a small magnetic field of H_{c1}, leading to the 1/2 plateau at which the spins on the Ni2 sites are almost polarized. For classical Ni2 ions, the magnetization process would be dynamic, depending on temperature and field sweep rate [see Fig. 2(a)]. On the contrary, the Ni1 ions form strong antiferromagnetically coupled dimer with a large spin gap (Δ–J_3). A large magnetic field is required to drive the Ni1 dimer to experience two quantum phase transitions within H_{c2}–H_{c3} and H_{c4}–H_{c5} preceding the magnetic saturation, resulting in quantum 1/2 plateau. The energy levels for the isolated Ni1 dimer are plotted in Fig. 2(c). Clearly, the 1/2 plateau is caused by the gaps between the states $|S_d, m_z\rangle = |0, 0\rangle$, $|1, 1\rangle$, and $|2, 2\rangle$,where S_d is the total spin and the z component $m_z = -S_d, \ldots, S_d$. Eventually, the magnetization process of the Ni1 dimer is superposed on that of the Ni2 monomers, giving rise to the 1/2 and 3/4-like plateaus of $Ni_2V_2O_7$. The classical and quantum magnetism coexist in $Ni_2V_2O_7$.

With the "dimer+monomer" model, magnetic susceptibility $\chi(T)$ curve is calculated. Figure 4 shows a comparison between the calculated and the experimental $\chi(T)$ curves. As expected, the dimer term exhibits a broad maximum around 70 K, but its value is too small (due to large J_3) to have a substantial contribution to the total $\chi(T)$. This finding proves that the dimerization cannot be revealed without the full magnetization process that is obtained by ultrahigh magnetic fields exceeding 100 T.

The experimental $M(H)$ curves at 4.5 and 2.2 K [Fig. 2(a)] always exhibit a certain slope in the gapless regions of H_{c2}–H_{c3} and H_{c4}–H_{c5}. In addition to the thermal effect, this feature reflects the presence of inter-dimer interactions, which

may results in the supersolid states proposed by Momoi and Totuska [41]. In the famous S-1/2 orthogonal-dimer antiferromagnet $SrCu_2(BO_3)_2$, except for a sequence of magnetization plateaus at 1/2, 2/5, 1/3, 1/4, 1/6, 2/15, and 1/8 of the saturation, various supersolid phases between these plateaus were observed due to the localized triplets in the square magnetic unit cells [18,42,43]. Such a supersolid state, in which a spin density wave and superfluid of spins coexist, is formed by deforming or rotating the spins in the plateau phases, leading to a smooth increase in magnetization. For $Ni_2V_2O_7$, the Ni1 dimers are periodically arranged to form square lattice in the bc plane [Fig. 1(b)]. With the weak interactions (J_4) between these dimers, excited triplets ($S_d = 1$) or even quintets ($S_d = 2$) can be localized, forming superlattices in the bc plane. Thus additional plateaus and supersolid states are expected to appear within H_{c2}–H_{c3} and H_{c4}–H_{c5}. For example, assuming that one half of the dimers are in the singlet state and the rest in the triplet state, a 5/8 plateau is expected. The multipeak structure is seen within H_{c2}–H_{c3} and H_{c4}–H_{c5} in dM/dH curve at 120 T [Fig. 2(a)], but not in the 104 T data (not shown here). The plateau width might be tiny and hard to be detected, similar to the case of $SrCu_2(BO_3)_2$. Recognition of the tiny plateaus and supersolid states within H_{c2}–H_{c3} and H_{c4}–H_{c5} awaits further ultralow-temperature experiments.

Finally, we note that the experimental curve is lower than the theoretical 3/4 plateau, which means that only 85% of the dimers are in the triplet state and the rest remain in the singlet state. Ideally, if all the dimers are in the triplet state between H_{c3} and H_{c4}, then a standard 3/4 plateau (i.e., 1/2 plateau of the dimer) forms.

IV. CONCLUSION

In summary, a 1/2 magnetization plateau within 11.7–34.8 T and a 3/4-like plateau within 55.6–87.0 T are observed in magnetic field of up to 120 T for $Ni_2V_2O_7$. With the DFT, ED and QMC simulations, the magnetization process can be described satisfactorily, which yields main exchange interactions—the intrachain $J_1/k_B = -1.0$ K, $J_2/k_B = 6.3$ K, and the interchain $J_3/k_B = -78.5$ K. Thus the skew chain $Ni_2V_2O_7$ can be described by a "dimer+monomer" model: the 1/2 plateau is due to weakly coupled Ni2 monomers, while 3/4-like plateau is the result of dimerization of Ni1 ions originating from large overlap of 3d-orbital along the Ni1-Ni1 bond. The supersolid phases from Ni1 dimers are expected to exist in $Ni_2V_2O_7$. Our results are expected to arouse continuous experimental and theoretical interests in low-dimensional quantum magnets.

ACKNOWLEDGMENTS

This work was supported by the National Natural Science Foundation of China (Grant Nos. U20A2073 and 11874023).

[1] S. V. Streltsov and D. I. Khomskii, Phys. Rev. B **77**, 064405 (2008).
[2] H. F. Pen, J. van den Brink, D. I. Khomskii, and G. A. Sawatzky, Phys. Rev. Lett. **78**, 1323 (1997).
[3] J. P. Sheckelton, J. R. Neilson, D. G. Soltan, and T. M. McQueen, Nat. Mater **11**, 493 (2012).
[4] J. Carrasquilla, G. Chen, and R. G. Melko, Phys. Rev. B **96**, 054405 (2017).
[5] M. Schmidt, W. Ratcliff, P. G. Radaelli, K. Refson, N. M. Harrison, and S. W. Cheong, Phys. Rev. Lett. **92**, 056402 (2004).
[6] O. Janson, S. Furukawa, T. Momoi, P. Sindzingre, J. Richter, and K. Held, Phys. Rev. Lett. **117**, 037206 (2016).
[7] A. Ikeda, S. Furukawa, O. Janson, Y. H. Matsuda, S. Takeyama, T. Yajima, Z. Hiroi, and H. Ishikawa, Phys. Rev. B **99**, 140412(R) (2019).
[8] A. Paul, C. M. Chung, T. Birol, and H. J. Changlani, Phys. Rev. Lett. **124**, 167203 (2020).
[9] D. I. Khomskii, T. Mizokawa, and S. V. Streltsov, Phys. Rev. Lett. **127**, 049701 (2021).
[10] D. I. Khomskii and S. V. Streltsov, Chem. Rev. **121**, 2992 (2021).
[11] N. Terada, Y. Narumi, K. Katsumata, T. Yamamoto, U. Staub, K. Kindo, M. Hagiwara, Y. Tanaka, A. Kikkawa, H. Toyokawa, T. Fukui, R. Kanmuri, T. Ishikawa, and H. Kitamura, Phys. Rev. B **74**, 180404(R) (2006).
[12] Y. Shirata, H. Tanaka, A. Matsuo, and K. Kindo, Phys. Rev. Lett. **108**, 057205 (2012).
[13] T. Ono, H. Tanaka, H. Aruga Katori, F. Ishikawa, H. Mitamura, and T. Goto, Phys. Rev. B **67**, 104431 (2003).
[14] H. Ishikawa, M. Yoshida, K. Nawa, M. Jeong, S. Krämer, M. Horvatić, C. Berthier, M. Takigawa, M. Akaki, A. Miyake, M. Tokunaga, K. Kindo, J. Yamaura, Y. Okamoto, and Z. Hiroi, Phys. Rev. Lett. **114**, 227202 (2015).
[15] F. Bert, D. Bono, P. Mendels, F. Ladieu, F. Duc, J. C. Trombe, and P. Millet, Phys. Rev. Lett. **95**, 087203 (2005).
[16] H. Yoshida, J. Yamaura, M. Isobe, Y. Okamoto, G. J. Nilsen, and Z. Hiroi, Nat. Commun. **3**, 860 (2012).
[17] E. Kermarrec, R. Kumar, G. Bernard, R. Hénaff, P. Mendels, F. Bert, P. L. Paulose, B. K. Hazra, and B. Koteswararao, Phys. Rev. Lett. **127**, 157202 (2021).
[18] Y. H. Matsuda, N. Abe, S. Takeyama, H. Kageyama, P. Corboz, A. Honecker, S. R. Manmana, G. R. Foltin, K. P. Schmidt, and F. Mila, Phys. Rev. Lett. **111**, 137204 (2013).
[19] Z. Wang, D. L. Quintero-Castro, S. Zherlitsyn, S. Yasin, Y. Skourski, A. T. M. N. Islam, B. Lake, J. Deisenhofer, and A. Loidl, Phys. Rev. Lett. **116**, 147201 (2016).
[20] Y. Okamoto, D. Nakamura, A. Miyake, S. Takeyama, M. Tokunaga, A. Matsuo, K. Kindo, and Z. Hiroi, Phys. Rev. B **95**, 134438 (2017).
[21] E. E. Sauerbrei, R. Faggiani, and C. Calvo, Acta Crystallogr., Sect. B: Struct. Sci. **30**, 2907 (1974).
[22] Z. He, J. I. Yamaura, Y. Ueda, and W. D. Cheng, Phys. Rev. B **79**, 092404 (2009).
[23] Z. W. Ouyang, Y. C. Sun, J. F. Wang, X. Y. Yue, R. Chen, Z. X. Wang, Z. Z. He, Z. C. Xia, Y. Liu, and G. H. Rao, Phys. Rev. B **97**, 144406 (2018).
[24] R. Chen, J. F. Wang, Z. W. Ouyang, Z. Z. He, S. M. Wang, L. Lin, J. M. Liu, C. L. Lu, Y. Liu, C. Dong, C. B. Liu, Z. C. Xia,

A. Matsuo, Y. Kohama, and K. Kindo, Phys. Rev. B **98**, 184404 (2018).
[25] T. Tonegawa, T. Nakao, and M. Kaburagi, J. Phys. Soc. Jpn. **65**, 3317 (1996).
[26] Y. Narumi, K. Kindo, M. Hagiwara, H. Nakano, A. Kawaguchi, K. Okunishi, and M. Kohno, Phys. Rev. B **69**, 174405 (2004).
[27] X. Yan, W. Li, Y. Zhao, S.-J. Ran, and G. Su, Phys. Rev. B **85**, 134425 (2012).
[28] Y. C. Sun, Z. W. Ouyang, J. F. Wang, Z. X. Wang, Z. C. Xia, and G. H. Rao, Eur. Phys. J. Plus **131**, 343 (2016).
[29] S. Takeyama, R. Sakakura, Y. H. Matsuda, A. Miyata, and M. Tokunaga, J. Phys. Soc. Jpn. **81**, 014702 (2012).
[30] X.-G. Zhou, Y. Yao, Y. H. Matsuda, A. Ikeda, A. Matsuo, K. Kindo, and H. Tanaka, Phys. Rev. Lett. **125**, 267207 (2020).
[31] P. Blaha, K. Schwarz, F. Tran, R. Laskowski, G. K. H. Madsen, and L. D. Marks, J. Chem. Phys. **152**, 074101 (2020).
[32] M. T. Czyżyk and G. A. Sawatzky, Phys. Rev. B **49**, 14211 (1994).
[33] See Supplemental Material at http://link.aps.org/supplemental/10.1103/PhysRevB.106.184409 for details on DFT calculations, ED and quantum Monte Carlo simulations.
[34] J. P. Perdew, K. Burke, and M. Ernzerhof, Phys. Rev. Lett. **77**, 3865 (1996).
[35] O. F. Syljuåsen and A. W. Sandvik, Phys. Rev. E **66**, 046701 (2002).
[36] A. W. Sandvik, Phys. Rev. B **59**, R14157(R) (1999).
[37] A. F. Albuquerque, F. Alet, P. Corboz *et al.*, J. Magn. Magn. Mater. **310**, 1187 (2007).
[38] F. Alet, S. Wessel, and M. Troyer, Phys. Rev. E **71**, 036706 (2005).
[39] Z. Hiroi, H. Ishikawa, H. Yoshida, J. Yamaura, and Y. Okamoto, Inorg. Chem. **58**, 11949 (2019).
[40] L. Yin, Z. W. Ouyang, J. F. Wang, X. Y. Yue, R. Chen, Z. Z. He, Z. X. Wang, Z. C. Xia, and Y. Liu, Phys. Rev. B **99**, 134434 (2019).
[41] T. Momoi and K. Totsuka, Phys. Rev. B **62**, 15067 (2000).
[42] H. Kageyama, K. Onizuka, T. Yamauchi, Y. Ueda, S. Hane, H. Mitamura, T. Goto, K. Yoshimura, and K. Kosuge, J. Phys. Soc. Jpn. **68**, 1821 (1999).
[43] M. Takigawa, M. Horvatić, T. Waki, S. Krämer, C. Berthier, F. Lévy-Bertrand, I. Sheikin, H. Kageyama, Y. Ueda, and F. Mila, Phys. Rev. Lett. **110**, 067210 (2013).